electronics

MDPI

Article

Estimation of the State of Charge of Lithium Batteries Based on Adaptive Unscented Kalman Filter Algorithm

Jiechao Lv, Baochen Jiang, Xiaoli Wang *, Yirong Liu and Yucheng Fu

School of Mechanical, Electrical and Information Engineering, Shandong University, Weihai 264209, China; lvjiechao@mail.sdu.edu.cn (J.L.); jbc@sdu.edu.cn (B.J.); lyr@mail.sdu.edu.cn (Y.L.); whj3105@126.com (Y.F.)

* Correspondence: wxl@sdu.edu.cn; Tel.: +86-138-6302-6640

Received: 24 July 2020; Accepted: 31 August 2020; Published: 2 September 2020

Abstract: The state of charge (SOC) estimation of the battery is one of the important functions of the battery management system of the electric vehicle, and the accurate SOC estimation is of great significance to the safe operation of the electric vehicle and the service life of the battery. Among the existing SOC estimation methods, the unscented Kalman filter (UKF) algorithm is widely used for SOC estimation due to its lossless transformation and high estimation accuracy. However, the traditional UKF algorithm is greatly affected by system noise and observation noise during SOC estimation. Therefore, we took the lithium cobalt oxide battery as the analysis object, and designed an adaptive unscented Kalman filter (AUKF) algorithm based on innovation and residuals to estimate SOC. Firstly, the second-order RC equivalent circuit model was established according to the physical characteristics of the battery, and the least square method was used to identify the parameters of the model and verify the model accuracy. Then, the AUKF algorithm was used for SOC estimation; the AUKF algorithm monitors the changes of innovation and residual in the filter and updates system noise covariance and observation noise covariance in real time using innovation and residual, so as to adjust the gain of the filter and realize the optimal estimation. Finally came the error comparison analysis of the estimation results of the UKF algorithm and AUKF algorithm; the results prove that the accuracy of the AUKF algorithm is 2.6% better than that of UKF algorithm.

Keywords: SOC; second-order RC equivalent circuit model; system noise covariance; observation noise covariance; AUKF

1. Introduction

In recent years, with the escalating energy crisis and environmental problems, low-pollution, high-efficiency electric vehicles (EVs) have become a hot spot in the automotive industry. Lithium-ion batteries have the characteristics of small size, light weight, high energy density, large output power and high safety performance, and have become the first choice for energy storage devices of EVs [1–3]. State of charge (SOC) is used to directly reflect the remaining capacity of the battery, which is an important basis for the vehicle control system to formulate an optimal energy management strategy. SOC is an important battery performance parameter; accurate estimation of SOC is of great significance to improve battery safety performance, extend battery life and ensure reliable operation of battery system [4,5].

At present, the commonly used SOC estimation methods for lithium batteries include the ampere-hour integration method, the open circuit voltage method, the neural network method, the particle filter algorithm and the Kalman Filter (KF) method. Among them, the ampere-hour integration method estimates the SOC of the battery by accumulating the amounts of charge and

discharge, and at the same time compensates the estimated SOC according to the self-discharge rate [6,7]. The ampere-hour integration method is relatively simple; it can dynamically estimate the battery SOC, but the current integration needs to obtain the initial SOC value, and the battery current must be accurately collected, which leads to the accumulation of SOC estimation errors over time. In practical applications, the ampere-hour integration method is usually used in combination with other methods to improve the estimation accuracy.

The open circuit voltage method is to indirectly fit the corresponding relationship between the open circuit voltage and the battery SOC, according to the relationship between the open circuit voltage of the battery and the lithium ion concentration in the battery [8,9]. The open circuit voltage method requires the battery to be placed statically for a long time to obtain a stable terminal voltage. Therefore, the open circuit voltage method cannot be used to estimate the SOC of the battery online in real time.

The neural network method is an algorithm for simulating the human brain and its neurons to deal with nonlinear systems, without in-depth study of the internal structure of the battery. The neural network method only needs to extract a large number of input and output samples from the target battery in accordance with its working characteristics in advance, and input it into the system established by using this method, and the SOC of the battery can be obtained [10,11]. The neural network method has high operational complexity, and it needs to extract a large amount of comprehensive target sample data to train the system. The input training data and training method will affect the accuracy of SOC estimation to a large extent.

The particle filtering is a process of approximating the probability density function by finding a set of random samples propagating in the state space, replacing the integral operation with the sample mean and then obtaining the minimum variance estimation process of the system state [12,13]. The particle filter algorithm is suitable for nonlinear non-Gaussian systems. The more particles used, the more accurate the SOC estimation value. However, as the number of particles increases, the calculation load increases. Additionally, particle degradation and insufficient particle diversity will seriously affect the SOC estimation results.

The KF algorithm is a type of optimized autoregressive data filtering algorithm. The essence of the algorithm is to make an optimal estimate of complex dynamic systems according to the principle of least mean square error [14–18]. KF algorithm overcomes the serious shortcoming of the current integration dependence on the initial value, and does not require a large number of sample data, and can be used to estimate the battery SOC online. In the SOC estimation of electric vehicle power batteries with complex operating conditions, the KF algorithm has a significant application value, and has become a hot spot in the research of battery SOC estimation algorithms in recent years [19,20]. The KF is an algorithm that uses the linear system state equation to observe the system input and output data to optimally estimate the state of the system.

Since KF cannot solve the problem of nonlinear systems, study [21] used the extended Kalman filter (EKF) to expand nonlinear systems into linear systems using Taylor series. EKF is an extended form of the standard Kalman filter in non-linear situations, and it is a highly efficient recursive filter. The basic idea of EKF is to use Taylor series expansion to linearize the nonlinear system, and then use the Kalman filter framework to filter the signal, so it is a sub-optimal filter. EKF algorithm is used for SOC estimation in battery management systems (BMSs), and has achieved good results in SOC estimation based on equivalent circuit model [22–24]. Although this method solves the nonlinear problem, it ignores high-order terms and increases linear errors, which may cause the filter to diverge.

Reference [25] used the unscented Kalman filter (UKF) to perform an unscented transformation on a nonlinear system without ignoring higher-order terms, which improved the accuracy of the estimation. UKF is a combination of unscented transform and standard Kalman filter system. Through unscented transform, the nonlinear system equation is suitable for the standard Kalman system under the linear assumption. The basic idea of UKF is Kalman filtering and unscented transform, which can effectively overcome the problems of low accuracy and poor stability of EKF estimation. As high-order terms are not ignored, the calculation accuracy of nonlinear distribution statistics is high. However,

the uncertainty of the battery model and system noise is not considered. Uncertainty of model noise and system noise will lead to increased error, slow convergence speed and filter divergence. Reference [26] introduces adaptive filtering on the basis of UKF, and replaces system noise covariance and observation noise covariance of UKF with adaptive-filter-estimated system noise covariance and observation noise covariance, respectively. In order to update the system error and the observation error in real time, the filtering effect is relatively good, but the adaptive filtering cannot truly reflect the system noise and the observation noise error, so it can be further improved.

In the traditional UKF algorithm [27,28], the system noise covariance and the observation noise covariance are usually set as constants, which cannot truly reflect the dynamic characteristics of noise, and have a certain influence on the accuracy of SOC estimation. In view of the shortcomings of the traditional UKF algorithm in the case of low model accuracy and uncertain noise, we designed an adaptive unscented Kalman filter (AUKF). The AUKF algorithm monitors the dynamic changes of innovation and residual in the filter in real time; corrects the system noise covariance and observation noise covariance in real time; and adjusts the filter gain to improve the estimation accuracy.

The organizational structure of this paper is as follows. In Section 1, the common methods for battery SOC estimation are introduced, and the methods designed in this paper are briefly introduced. In Section 2, the second-order RC equivalent circuit model is established, the parameters are identified and the accuracy of the model is verified. In Section 3, the traditional UKF algorithm and the AUKF algorithm designed in this paper are introduced. In Section 4, the convergence speed and estimation accuracy of the UKF algorithm and AUKF algorithm are compared through experiments. In Section 5, the work and research results of this paper are summarized.

2. Lithium Battery Model

2.1. The Second-Order RC Equivalent Circuit Model of a Lithium-Ion Battery

An accurate battery model is the basis for SOC estimation. Battery models can be roughly divided into electrochemical models [29,30], mathematical models [31] and equivalent circuit models [32,33]. Although the accuracy of the electrochemical model is high, the structure is complex and difficult to implement, and it is not suitable for modeling actual working conditions. The mathematical model has a simple structure and is easy to calculate, but it is difficult to describe the external characteristics of the battery. Considering the complexity and accuracy of the battery model, this paper uses a second-order RC equivalent circuit model [34]; the schematic diagram is shown in Figure 1.

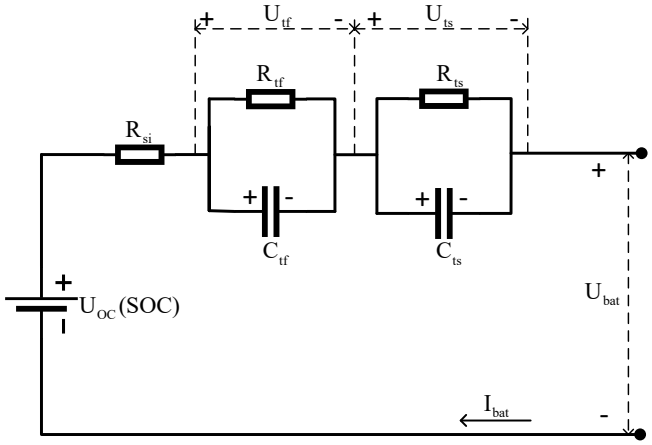

Figure 1. Schematic diagram of the second-order RC equivalent circuit.

In Figure 1, $U_{OC}(SOC)$ represents the battery open circuit voltage related to SOC; I_{bat} represents the open circuit current of the battery, and the discharge current is a positive value; U_{bat} represents the battery terminal voltage; R_{si} represents the ohmic internal resistance of the battery; R_{tf} and C_{tf}

represent the polarization resistance and polarization capacitance of the battery respectively; R_{ts} and C_{ts} represent concentration polarization resistance and concentration polarization capacitance respectively; U_{tf} and U_{ts} represent the voltage across the polarization capacitance and the concentration polarization capacitance, respectively. According to Kirchhoff's law, the state equation and output equation of the equivalent circuit can be obtained:

$$\begin{cases} \frac{dU_{tf}}{dt} = -\frac{U_{tf}}{R_{tf}C_{tf}} + \frac{I_{bat}}{C_{tf}} \\ \frac{dU_{ts}}{dt} = -\frac{U_{ts}}{R_{ts}C_{ts}} + \frac{I_{bat}}{C_{ts}} \\ \frac{dSOC}{dt} = -\frac{I_{bat}}{Q_{bat}} \end{cases} \tag{1}$$

$$U_{bat} = U_{OC}(SOC) - R_{si}I_{bat} - U_{tf} - U_{ts} \tag{2}$$

where Q_{bat} is the rated capacity of the battery.

2.2. Parameter Identification

Parameter identification technology is a technology that combines theoretical models and experimental data for prediction. Parameter identification determines the parameter values of a group of models based on the model established by the experimental data, so that the numerical results calculated by the model can better fit the test data, so that the unknown process can be predicted.

In this section, we identify the parameters through the voltage response curve of battery discharge and combine Equations (1) and (2); the parameters to be identified are $R_{si}, R_{tf}, C_{tf}, R_{ts}, C_{ts}$ and function relationship $U_{OC}(SOC)$.

The cell model used in the experiment in this paper was the SAMSUNG 30Q INR18650 power lithium cell. The specific parameters of the cell are shown in Table 1. The experimental object of this paper is a battery composed of 10 parallel lithium cobalt oxide cells. The battery was discharged by 1 C pulsed for 3 min, placed statically for 2 h and discharged to the cut-off voltage in cycles. The pulsed discharge voltage is shown in Figure 2a, and the pulsed discharge current is shown in Figure 2b.

Table 1. Power lithium cell parameters.

Parameter	Value
Cell model	SAMSUNG 30Q INR18650
Rated capacity	3000 mA h
Rated voltage	3.6 V
Discharge cut-off voltage	2.5 V
Weight	48.1 ± 1.5 g
Size	18.2 mm (D) × 65.0 mm (H)

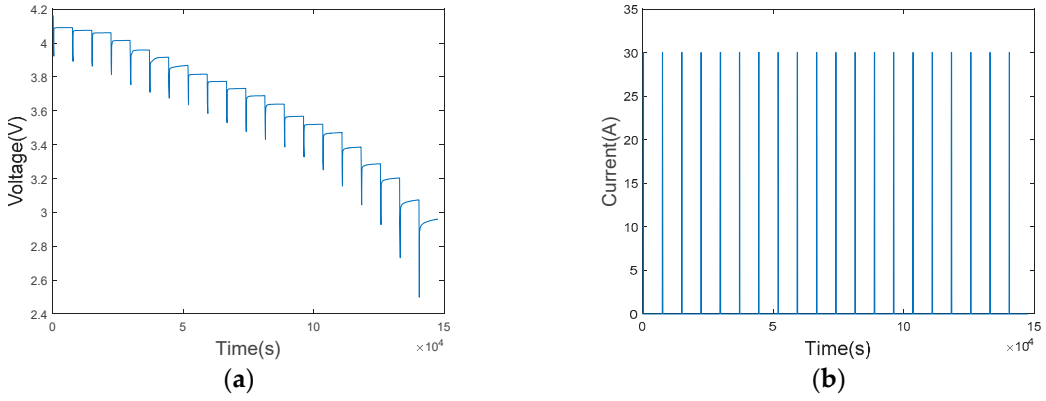

(**a**) (**b**)

Figure 2. Pulsed discharge current and voltage of the battery. (**a**) Battery pulsed discharge voltage. (**b**) Battery pulsed discharge current.

2.2.1. Parameter Identification of the Functional Relationship between U_{oc} and SOC

The battery SOC and open circuit voltage U_{oc} were obtained by the static method [35], and the corresponding values of SOC and open circuit voltage U_{oc} are shown in Table 2.

Table 2. U_{oc} and SOC corresponding relationship value.

U_{OC} (V)	SOC	U_{OC} (V)	SOC
4.1617	1	3.7317	0.5034
4.0913	0.9503	3.6892	0.4537
4.0749	0.9007	3.6396	0.4040
4.0606	0.8510	3.5677	0.3543
4.0153	0.8013	3.5208	0.3046
3.9592	0.7517	3.4712	0.2550
3.9164	0.7020	3.3860	0.2053
3.8687	0.6524	3.2880	0.1556
3.8163	0.6027	3.2037	0.1059
3.7735	0.5530	3.0747	0.0563

Use MATLAB to perform the least squares fitting of the data in Table 2 to obtain the equation of the functional relationship between U_{oc} and SOC; the equation is shown in Equation (3). The fitted relationship curve between U_{oc} and SOC is shown in Figure 3.

$$\begin{aligned} U_{OC}(SOC) = {} & 122.4786 * SOC^8 - 401.4734 * SOC^7 + 485.6818 * SOC^6 \\ & -239.2806 * SOC^5 + 3.7304 * SOC^4 + 44.9020 * SOC^3 - 19.8057 * SOC^2 \\ & +5.0932 * SOC + 2.8341 \end{aligned} \tag{3}$$

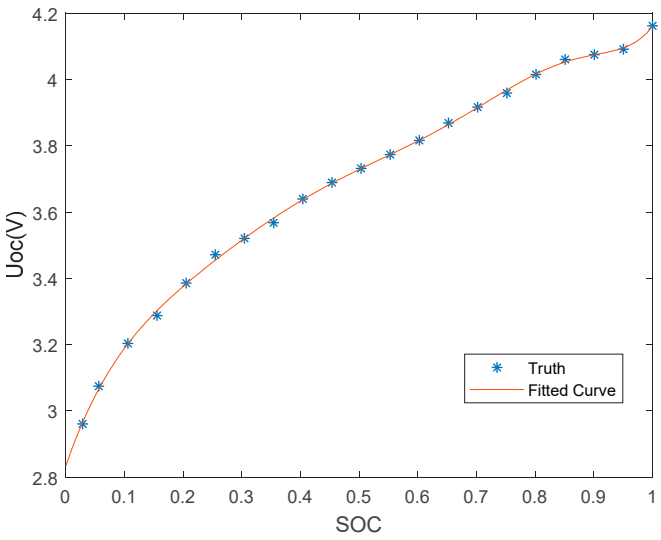

Figure 3. U_{oc}–SOC fitting curve.

2.2.2. Parameter Identification of Resistance and Capacitance

This paper combines the characteristics of resistance and capacitance, and analyzes the voltage response curve of the battery pulsed discharge to identify the resistance and capacitance. The partial discharge voltage diagram of the battery pulsed discharge is shown in Figure 4, and the battery voltage response curve can be divided into four stages:

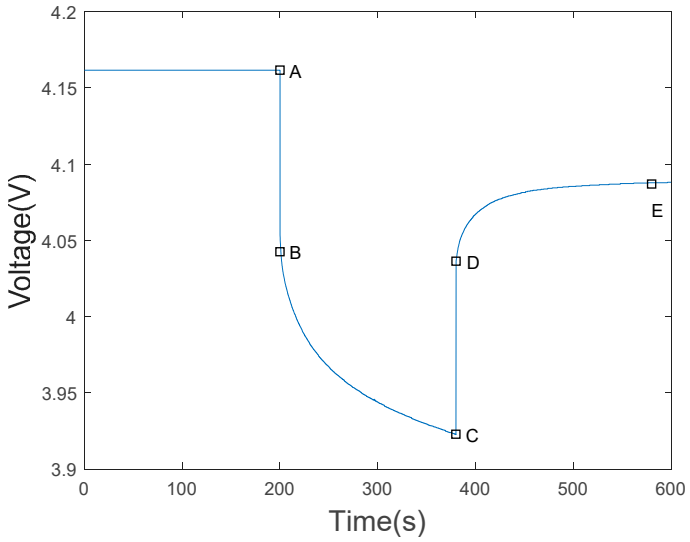

Figure 4. Partial enlargement of pulsed discharge voltage.

Section A-B: The battery turns from a static state to a discharged state, and the terminal voltage drops abruptly. From the second-order equivalent circuit diagram, it can be seen that U_{tf} and U_{ts} cannot be abruptly changed. The sudden drop in the voltage of section A-B is caused by the ohmic internal resistance R_{si}.

Section B-C: During the continuous discharge, electrochemical polarization and concentration polarization work together to make the voltage drop in the form of exponential changes. Before section B-C, U_{tf} and U_{ts} are zero, so section B-C can be regarded as a zero state response.

Section C-D: The battery discharge current disappears and the battery terminal voltage rises rapidly. It is the same as the section A-B. It can be considered that it is caused by the ohmic internal resistance R_{si}.

Section D-E: The battery is at rest. Due to the electrochemical polarization and concentration difference, the voltage is slowly increased. At this time, there is no current discharge, which can be regarded as zero input response.

According to the sections A-B and C-D in Figure 4, the ohmic internal resistance can be obtained:

$$R_{si} = \frac{(U_A - U_B) + (U_D - U_C)}{2I_{bat}} \tag{4}$$

where U_A, U_B, U_C, U_D are the battery terminal voltages corresponding to points A, B, C and D in Figure 4 respectively; I_{bat} is the discharge current of the battery.

Solving the differential equation according to Equation (1) gives Equation (5):

$$\begin{cases} U_{tf}(t) = U_{tf}(0)e^{-t/\tau_{tf}} + I_{bat}R_{tf}(1 - e^{-t/\tau_{tf}}) \\ U_{ts}(t) = U_{ts}(0)e^{-t/\tau_{ts}} + I_{bat}R_{ts}(1 - e^{-t/\tau_{ts}}) \end{cases} \tag{5}$$

where $\tau_{tf} = R_{tf}C_{tf}, \tau_{ts} = R_{ts}C_{ts}$ are the fast time constant and slow time constant respectively; $U_{tf}(0)$ and $U_{ts}(0)$ are the initial voltages across C_{tf}, C_{ts}, respectively.

According to Figure 4, the discharge current is zero in the DE segment, as a zero input response state. Taking point D as the starting moment, the zero input response expression of the RC loop can be obtained as shown in Equation (6):

$$\begin{cases} U_{tf} = U_{tf}(0)e^{-t/\tau_{tf}} \\ U_{ts} = U_{ts}(0)e^{-t/\tau_{ts}} \end{cases} \tag{6}$$

Combined with Equation (2), the battery output equation at zero input response is:

$$U_{bat}(t) = U_{OC}(SOC) - U_{tf}(0)e^{-t/\tau_{tf}} - U_{ts}(0)e^{-t/\tau_{ts}} \tag{7}$$

Equation (7) can be simplified:

$$U_{bat}(t) = U_{OC}(SOC) - b_1e^{-\lambda_1 t} - b_2e^{-\lambda_2 t} \tag{8}$$

where $\tau_{tf} = \frac{1}{\lambda_1}, \tau_{ts} = \frac{1}{\lambda_2}, U_{tf}(0) = b_1, U_{ts}(0) = b_2$.

By using Equation (8) as the fitting function, and using MATLAB to perform the least squares fitting on the DE segment in Figure 4, the value of $b_1, b_2, \lambda_1, \lambda_2$ can be obtained.

According to the BC segment in Figure 4, it can be regarded as a zero state response. Taking point B as the initial moment, the expression of the zero state response of the RC loop can be obtained as shown in Equation (9):

$$\begin{cases} U_{tf}(t) = I_{bat}R_{tf}(1 - e^{-t/\tau_{tf}}) \\ U_{ts}(t) = I_{bat}R_{ts}(1 - e^{-t/\tau_{ts}}) \end{cases} \tag{9}$$

Combined with Equation (2), the battery output equation at zero state response is:

$$U_{bat}(t) = U_{OC}(SOC) - I_{bat}R_{si} - I_{bat}R_{tf}(1 - e^{-t/\tau_{tf}}) - I_{bat}R_{ts}(1 - e^{-t/\tau_{ts}}) \tag{10}$$

Take τ_{tf}, τ_{ts} obtained by the Equation (8) fitting into Equation (10), use Equation (10) as the fitting function and use MATLAB to perform the least squares fitting of the BC segment in Figure 4; that will provide the values of a_1, a_2, and then the value of R_{tf}, R_{ts} is obtained:

$$\begin{cases} R_{tf} = \frac{a_1}{I_{bat}} \\ R_{ts} = \frac{a_2}{I_{bat}} \end{cases} \tag{11}$$

According to $\tau_{tf} = R_{tf}C_{tf}, \tau_{ts} = R_{ts}C_{ts}$, the value of C_{tf}, C_{ts} can be obtained.

According to the battery discharge voltage curve and battery characteristics, the results of identifying the parameters of the battery model by using the least square method in MATLAB are shown in Figure 5.

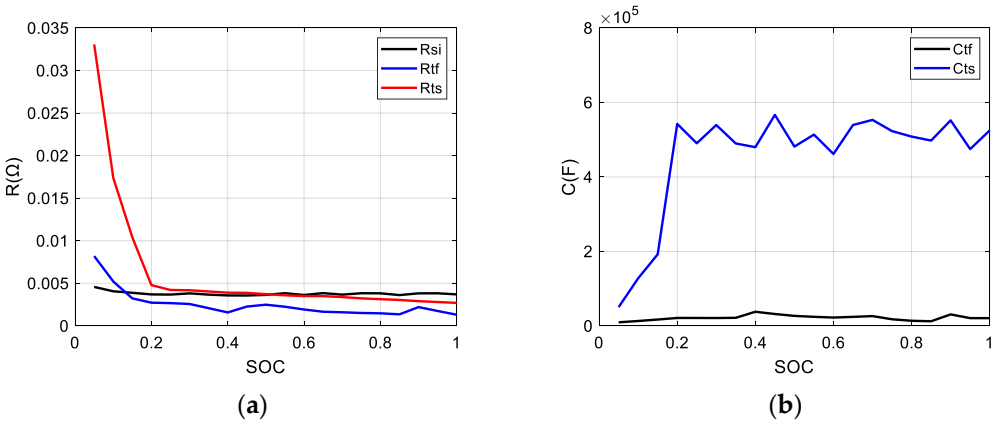

Figure 5. Result of parameter identification. (**a**) The value of the resistance. (**b**) The value of the capacitor.

Figure 5 shows the change of battery resistance and capacitance with SOC when the battery is discharged with constant current pulsed at a constant temperature of 25 °C. When the battery SOC value is between 0% and 20%, the resistance and capacitance values change greatly, and when the battery SOC value is between 20% and 100%, the resistance and capacitance values change relatively

little. Considering that the lower limit SOC value of battery in the actual working environment is 20%, this paper takes the average value of the resistance and capacitance of the battery's SOC in the range of 20–100% as the battery parameters for the subsequent SOC estimation experiment.

The average value of the resistance and capacitance of the battery with SOC in the range of 20–100% is shown in Table 3.

Table 3. Lithium-ion battery parameter identification results.

R_{si} (Ω)	R_{tf} (Ω)	R_{ts} (Ω)	C_{tf} (F)	C_{ts} (F)
0.0037	0.0019	0.0035	23,340	501,270

2.2.3. Verifying the Battery Model

Take the battery parameters identified in Table 3 into Equations (1) and (2), use the pulsed discharge current as input and compare the output terminal voltage with the actual terminal voltage. The comparison between the true value of the battery terminal voltage and the model value is shown in Figure 6; the model error value of the battery terminal voltage is shown in Figure 7; and the relevant parameters of the model error are shown in Table 4.

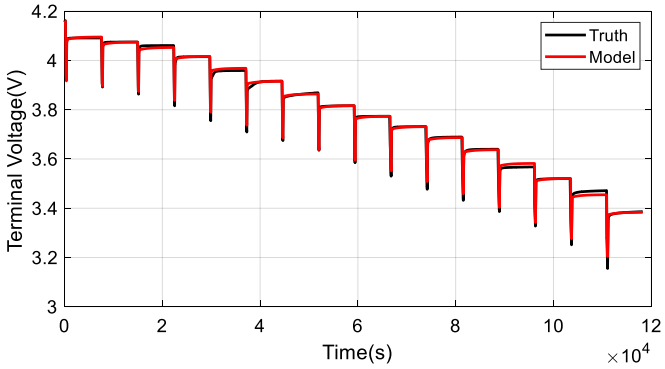

Figure 6. True value and modeled values of terminal voltage.

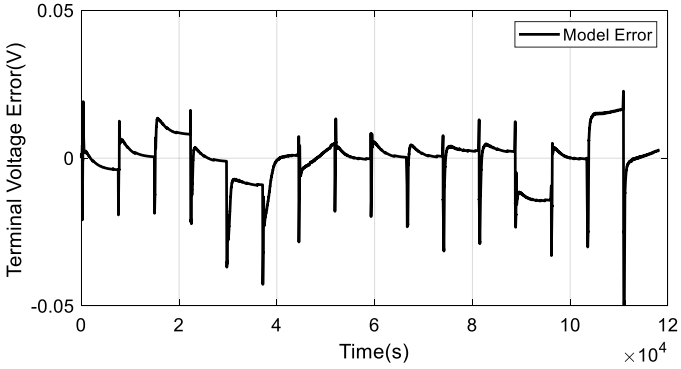

Figure 7. Terminal voltage error.

Table 4. Model error parameters.

Error Type	MAE	RMSE
Value	0.51%	0.8%

In Figure 6, the actual value of the battery terminal voltage is compared with the model value of the battery terminal voltage; the terminal voltage curve of the battery model is basically consistent with the true terminal voltage curve of the battery. In Figure 7, the terminal voltage error of the battery

model is shown; the terminal voltage error value of the battery model fluctuates around ±0.05 V. In Table 4, the terminal voltage error value of the battery model is calculated; the mean absolute error (MAE) of the terminal voltage of the battery model is 0.51%; the root mean square error (RMSE) of the terminal voltage of the battery model is 0.8%. The above results prove that the second-order RC equivalent circuit model of the battery designed in this paper is reasonable and reliable, and the battery model was able to be used in subsequent experiments.

3. Design of the SOC Estimation Algorithm

For a nonlinear system, the state equation and observation equation considering the system noise and observation noise are as shown in Equation (12):

$$\begin{cases} x_k = F(x_{k-1}, u_k) + w \\ y_k = G(x_{k-1}, u_k) + v \end{cases} \tag{12}$$

where k is the current moment, $F(x_{k-1}, u_k)$ is the nonlinear system state transition equation, $G(x_{k-1}, u_k)$ is the nonlinear observation equation, x_k is the state variable, u_k is the known input, y_k is the observation signal, w is the system noise and v is the observation noise.

According to the second-order equivalent circuit model of the battery, combining Equations (1) and (2), the discretized state equation and observation equation of the equivalent circuit model of the battery can be shown in Equation (13):

$$\begin{cases} \begin{bmatrix} U_{tf}(k) \\ U_{ts}(k) \\ SOC(k) \end{bmatrix} = \begin{bmatrix} e^{-\frac{\Delta t}{\tau_{tf}}} & 0 & 0 \\ 0 & e^{-\frac{\Delta t}{\tau_{ts}}} & 0 \\ 0 & 0 & 1 \end{bmatrix} \begin{bmatrix} U_{tf}(k-1) \\ U_{ts}(k-1) \\ SOC(k-1) \end{bmatrix} + \begin{bmatrix} R_{tf}(1-e^{-\frac{\Delta t}{\tau_{tf}}}) \\ R_{ts}(1-e^{-\frac{\Delta t}{\tau_{ts}}}) \\ -\frac{\Delta t}{Q_n} \end{bmatrix} I_{bat}(k) \\ U_{bat}(k) = U_{OC}(SOC) + [-1 \ -1 \ 0] \begin{bmatrix} U_{tf}(k) \\ U_{ts}(k) \\ SOC(k) \end{bmatrix} - I_{bat}(k) R_{si} \end{cases} \tag{13}$$

Equations (13) can be simplified to Equations (14):

$$\begin{cases} \boldsymbol{x}_k = \boldsymbol{A}_k \boldsymbol{x}_{k-1} + \boldsymbol{B}_k u_k \\ y_k = U_{OC}(SOC) + C\boldsymbol{x}_k - R_{si} u_k \end{cases} \tag{14}$$

where

$$\boldsymbol{x}_k = \begin{bmatrix} U_{tf}(k) \\ U_{ts}(k) \\ SOC(k) \end{bmatrix}, \boldsymbol{A}_k = \begin{bmatrix} e^{-\frac{\Delta t}{\tau_{tf}}} & 0 & 0 \\ 0 & e^{-\frac{\Delta t}{\tau_{ts}}} & 0 \\ 0 & 0 & 1 \end{bmatrix}, \boldsymbol{B}_k = \begin{bmatrix} R_{tf}(1-e^{-\frac{\Delta t}{\tau_{tf}}}) \\ R_{ts}(1-e^{-\frac{\Delta t}{\tau_{ts}}}) \\ -\frac{\Delta t}{Q_n} \end{bmatrix}, I_{bat}(k) = u_k, \ U_{bat}(k) = y(k), C = \begin{bmatrix} -1 & -1 & 0 \end{bmatrix}, R_{si}$$

is the ohmic internal resistance of the battery.

According to the KF principle, combining Equations (12) and (14), the first derivative of the nonlinear observation equation is calculated at the current state value, and the observation matrix can be obtained as Equation (15).

$$H_k = \frac{\partial G(x_k, u_k)}{\partial x_k} = \begin{bmatrix} -1 & -1 & \frac{\partial U_{oc}(SOC)}{\partial x} \end{bmatrix} \tag{15}$$

3.1. Design of the Unscented Kalman Filter Algorithm

The unscented Kalman filter (UKF) is a combination of the unscented transform (UT) and the standard Kalman filter system, and uses the unscented transform to adapt the nonlinear system

equations to the standard Kalman system under the linear assumption. UKF uses statistical linearization technology, which mainly linearizes the nonlinear function of random variables through linear regression of n Sigma points collected in the prior distribution. This linearization is more accurate than Taylor series linearization. The basic idea of UKF is Kalman filtering and unscented transform. Since UKF does not ignore high-order terms, it can effectively overcome the problems of low accuracy and poor stability of EKF estimation.

We conducted simulation experiments in MATLAB, and used the UKF algorithm to perform SOC estimation experiments under urban dynamometer driving schedule (UDDS) conditions, where the initial value $x_0 = [0\ 0\ 0.6]^T$, $P_0 = diag([10^{-5}, 10^{-5}, 10^{-3}])$, $Q = 10^{-7} \times eye(3)$, $R = 1$.

The UDDS operating conditions are shown in Figure 8. The estimation terminal voltage of the battery using the UKF algorithm for SOC estimation is shown in Figure 9. The SOC estimation results of the battery using the UKF algorithm for SOC estimation are shown in Figure 10.

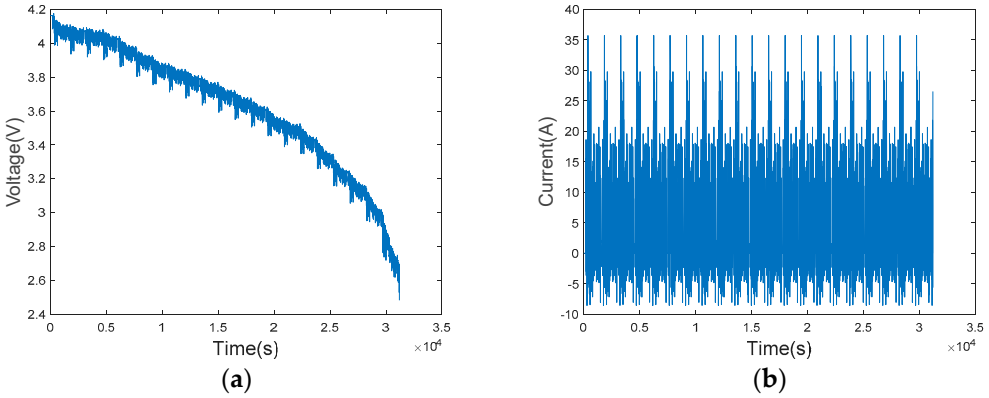

(**a**) (**b**)

Figure 8. UDDS operating conditions. (**a**) UDDS operating voltage. (**b**) UDDS operating current.

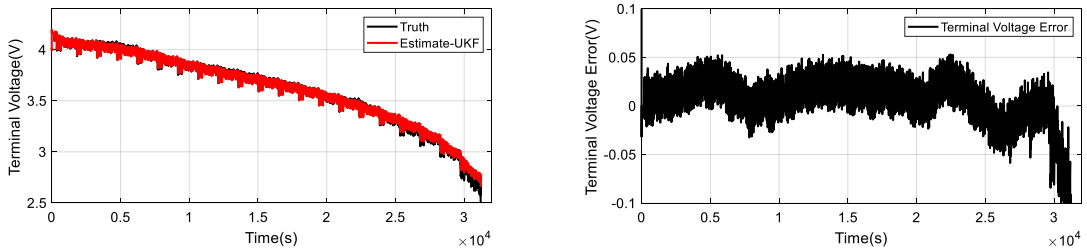

(**a**) (**b**)

Figure 9. The terminal voltage result of the battery was estimated using the UKF algorithm. (**a**) Estimated value and true value of terminal voltage of the battery. (**b**) Estimated error value of the terminal voltage of the battery.

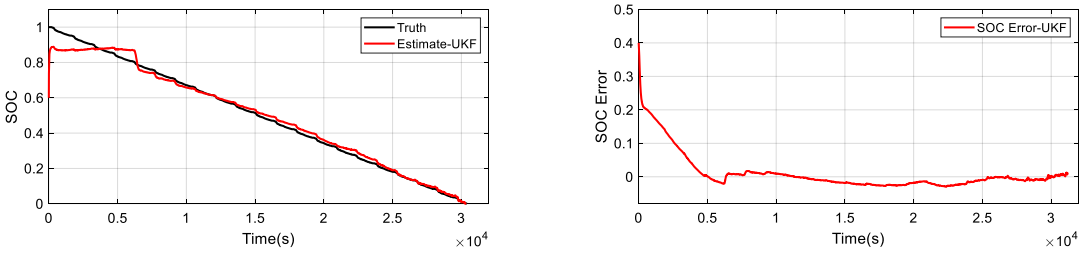

(**a**) (**b**)

Figure 10. The battery SOC estimation result was estimated using the UKF algorithm. (**a**) Estimated value and true value of SOC of the battery. (**b**) Estimated error value of SOC of the battery.

In Figure 9, the battery terminal voltage estimated by the UKF algorithm is shown. In Figure 9a, the estimated terminal voltage is compared with the true terminal voltage, and the estimated terminal voltage is not much different from the true terminal voltage. In Figure 9b, the terminal voltage error value of the battery fluctuates greatly. In Figure 10, the SOC of the battery estimated by UKF is shown. In Figure 10a, the estimated SOC of the battery differs greatly from the true value before 5000 seconds. In Figure 10b, the SOC estimation error of the battery just approached zero after 5000 seconds, and the convergence speed of the filter is slow.

3.2. Design of the Adaptive Unscented Kalman Filter Algorithm

The UKF algorithm uses UT to replace Taylor series expansion to transform a nonlinear system into a linear system, improving the accuracy of the algorithm. However, in the UKF algorithm, the system model noise and observation noise are set as constants, which cannot reflect the effect of real noise on the filter, which causes the SOC estimation error to increase or even diverge. In order to solve the above problems, we designed an AUKF algorithm; the algorithm is improved on the basis of the UKF algorithm; the algorithm monitors the change of innovation and residual in the filter in real time, and calculates the variance of innovation and residual by the moving window method. The system noise covariance is corrected in real time by the innovation variance, and the observation noise covariance is corrected in real time by the residual variance.

The AUKF algorithm process is as follows:

(1) Determine the initial value of state value $\hat{x}_0$ and the initial value of state error covariance P_0:

$$\hat{x}_0 = E[x_0] \tag{16}$$

$$P_0 = E\left[(x_0 - \hat{x}_0)(x_0 - \hat{x}_0)^T\right] \tag{17}$$

(2) Calculate Sigma point:

$$\begin{cases} x_k^0 = \hat{x}_{k-1} \\ x_{k-1}^i = \hat{x}_{k-1} + \sqrt{(L+\lambda)P_{k-1}}, i = 1, 2 \ldots L \\ x_{k-1}^i = \hat{x}_{k-1} - \sqrt{(L+\lambda)P_{k-1}}, i = L+1, L+2, \ldots 2L \end{cases} \tag{18}$$

where L is the length of the state vector, the length of the state vector in this paper is 3 and the weight value calculation is shown in Equation (19):

$$\begin{cases} \lambda = \alpha^2(L + k_i) - L \\ W_m^0 = \frac{\lambda}{L+\lambda}, W_m^i = \frac{1}{2(L+\lambda)}, i = 1, 2 \ldots 2L \\ W_c^0 = \frac{\lambda}{L+\lambda} + 1 - \alpha^2 + \beta, W_c^i = \frac{1}{2(L+\lambda)}, i = 1, 2 \ldots 2L \end{cases} \tag{19}$$

where $\alpha = 0.01, k_i = 0, \beta = 2$.

(3) Time update.

Update predicted status value $\overline{x}_k$:

$$x_{k|k-1}^i = F(x_{k-1}^i) \tag{20}$$

$$\overline{x}_k = \sum_{i=0}^{2L} W_m^i x_k^i \tag{21}$$

Update predicted observation $\overline{y}_k$.

$$y_{k|k-1}^i = G(x_{k|k-1}^i) \tag{22}$$

$$\overline{y}_k = \sum_{i=0}^{2L} W_m^i [G(x_{k|k-1}^i) + v] = \sum_{i=0}^{2L} W_m^i y_{k|k-1}^i \tag{23}$$

Update system covariance prediction value $P_{xx|k}$.

$$P_{xx|k} = \sum_{i=0}^{2L} (W_c^i (x_{k|k-1}^i - \overline{x}_k)(x_{k|k-1}^i - \overline{x}_k)^T) + Q_{k-1} \tag{24}$$

Calculate innovation value d_k and innovation variance value C_{d_k}.

$$d_k = y_k - \overline{y}_k \tag{25}$$

$$C_{d_k} = \begin{cases} \frac{k-1}{k} C_{d_{k-1}} + \frac{1}{k} d_k d_k{}^T & k \le W \\ \frac{1}{W} \sum\limits_{i=k-W+1}^{k} d_i d_i{}^T & k > W \end{cases} \tag{26}$$

Update system noise covariance Q_k.

$$Q_k = K_{k-1} C_{d_k} K_{k-1}{}^T \tag{27}$$

(4) Status update.
Update observation covariance prediction value $P_{yy|k}$.

$$P_{yy|k} = \sum_{i=0}^{2L} (W_c^i (y_{k|k-1}^i - \overline{y}_k)(y_{k|k-1}^i - \overline{y}_k)^T) + R_{k-1} \tag{28}$$

Update covariance $P_{xy|k}$.

$$P_{xy|k} = \sum_{i=0}^{2L} W_c^i (x_{k|k-1}^i - \overline{x}_k)(y_{k|k-1}^i - \overline{y}_k)^T \tag{29}$$

Calculate Kalman gain K_k.

$$K_k = \frac{P_{xy|k}}{P_{yy|k}} \tag{30}$$

Update estimated state value $\hat{x}_k$.

$$\hat{x}_k = \overline{x}_k + K_k (y_k - \overline{y}_k) \tag{31}$$

Update estimated observation $\hat{y}_k$.

$$\hat{y}_k = H_k \hat{x}_k \tag{32}$$

Update error covariance P_k.

$$P_k = P_{xx|k} - K_k P_{yy|k} K^T \tag{33}$$

Calculate the residual value r_k and the residual variance value C_{r_k}.

$$r_k = y_k - \hat{y}_k \tag{34}$$

$$C_{r_k} = \begin{cases} \frac{k-1}{k} C_{d_{r-1}} + \frac{1}{k} r_k r_k{}^T & k \le W \\ \frac{1}{W} \sum\limits_{i=k-W+1}^{k} r_i r_i{}^T & k > W \end{cases} \tag{35}$$

Update the observation noise covariance R_k.

$$R_k = C_{r_k} + H_k P_k {H_k}^T \tag{36}$$

The AUKF algorithm flow is shown in Figure 11.

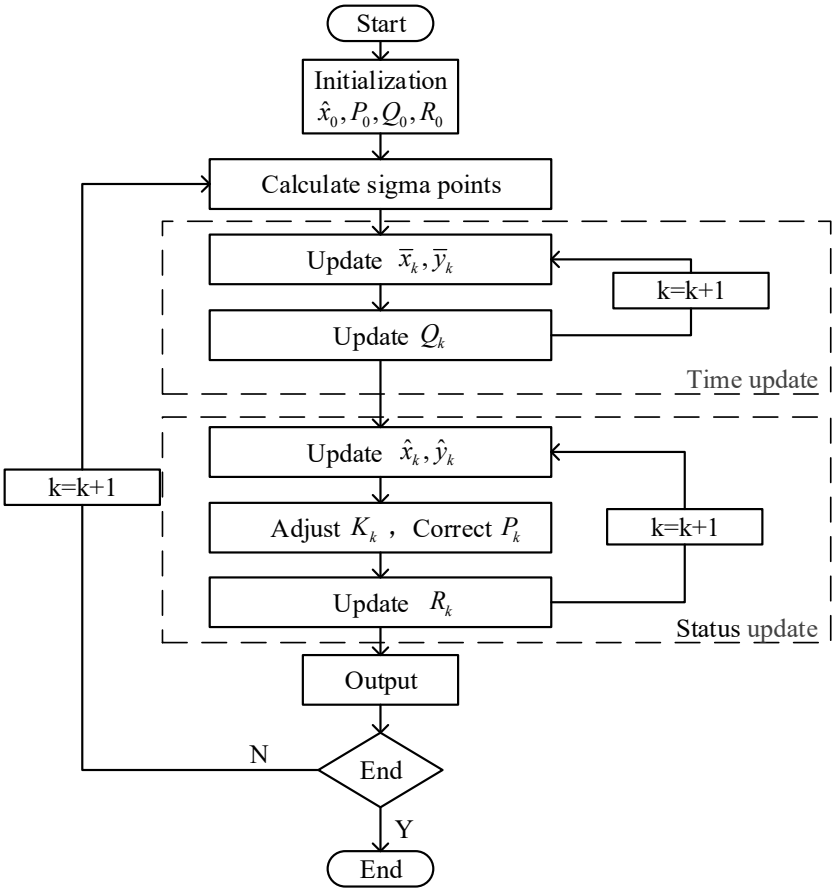

Figure 11. The flow of the AUKF algorithm.

3.2.1. Adaptive System Noise Covariance Q_k

From Equations (18), (21), (24), (27) and (33), it can be seen that when the Q_k value is too large, system covariance prediction $P_{xx|k}$ increases, so that the next predicted state value $\bar{x}_{k+1}$ becomes larger, which eventually leads to the estimated state value $\hat{x}_{k+1}$ being too large, which increases the SOC estimation error. Therefore, the system noise covariance Q_k can be updated in real time to correct the influence of the system error on the estimation result.

The innovation d_k at time k is defined as the difference between the actual observation value y_k and the predicted observation value $\bar{y}_k$. The expression of innovation is shown in Equation (37):

$$d_k = y_k - \bar{y}_k \tag{37}$$

According to the moving window method, the variance of innovation C_{d_k} is calculated as:

$$C_{d_k} = \begin{cases} \frac{k-1}{k} C_{d_{k-1}} + \frac{1}{k} d_k {d_k}^T & k \le W \\ \frac{1}{W} \sum_{i=k-W+1}^{k} d_i {d_i}^T & k > W \end{cases} \tag{38}$$

where W is the length of the moving window. Through the innovation variance C_{d_k}, the system noise covariance Q_k can be calculated [36] as shown in Equation (39),

$$Q_k = K_{k-1} C_{d_{k-1}} {K_{k-1}}^T \tag{39}$$

Since the system state variable has a dimension of 3, Q_k is a 3×3 symmetric matrix. This paper will represent Q_k as $Q_k = \begin{bmatrix} Q_{11} & Q_{12} & Q_{13} \\ Q_{21} & Q_{22} & Q_{23} \\ Q_{31} & Q_{32} & Q_{33} \end{bmatrix}$, where $Q_{12} = Q_{21}, Q_{13} = Q_{31}, Q_{23} = Q_{32}$. The Q_k value when using the AUKF algorithm to estimate the SOC in MATLAB is shown in Figure 12.

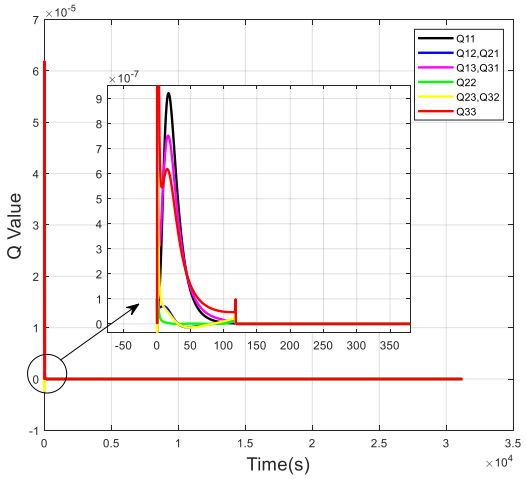

Figure 12. Q value of AUKF algorithm.

It can be seen from Figure 12 that since the initial value of SOC is uncertain, the system error is relatively large at this time, so the system noise covariance Q_k is relatively large. By calculating the value of innovation d_k, and then updating Q_k in real time to correct the error covariance P_k in time, the system noise is corrected in time, and the value of Q_k approaches to zero.

3.2.2. Adaptive Observation Noise Covariance R_k

From Equations (28), (30) and (33), it can be seen that the value of R_k determines the weight of the observation value to the estimated result. When the R_k value increases, the filter gain K_k decreases, resulting in the effect of the observation value on the estimated state value becoming smaller. Conversely, when the value of R_k decreases, the filter gain K_k will increase, which will increase the proportion of the observation value in the estimated state value. Therefore, the observation noise covariance R_k adjusts the Kalman gain K_k in real time to change the proportion of the predicted observation value in the estimation result, thereby reducing the influence of the observation noise on the estimation result.

The residual r_k at time k is defined as the difference between the actual observation value y_k and the estimated observation value $\hat{y}_k$. The expression of the residual is shown in Equation (40):

$$r_k = y_k - \hat{y}_k \tag{40}$$

According to the moving window method, the variance of residual C_{r_k} is calculated as:

$$C_{r_k} = \begin{cases} \frac{k-1}{k} C_{r_{k-1}} + \frac{1}{k} r_k {r_k}^T & k \le W \\ \frac{1}{W} \sum_{i=k-W+1}^{k} r_i {r_i}^T & k > W \end{cases} \tag{41}$$

Through the residual variance C_{r_k}, the observation noise covariance R_k can be calculated [37] as shown in Equation (42),

$$R_k = C_{r_k} + H_k P_{k-1} {H_k}^T \tag{42}$$

The R_k value when using the AUKF algorithm to estimate the SOC in MATLAB is shown in the Figure 13.

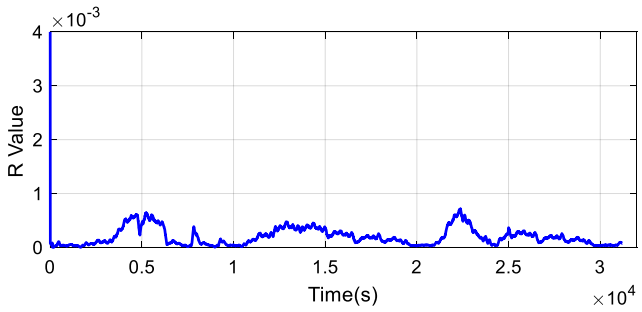

Figure 13. R value of AUKF algorithm.

It can be seen from Figure 13 that the value of R_k fluctuates in a small range. The residual r_k calculates the difference between the actual observation value and the estimated observation value, and then realizes the real-time update of R_k, and then adjusts the Kalman gain K_k to achieve the optimal estimation.

4. Comparison of SOC Estimation Algorithms

The battery SOC was estimated using the unscented Kalman filter algorithm; Q_k and R_k in the adaptive unscented Kalman filter algorithm were analyzed and simulated—see Section 3. In this section, we describe how the AUKF algorithm was used to estimate the battery SOC under different load cycles and different initial SOC values. The results of SOC estimation using AUKF algorithm and the results of SOC estimation using UKF algorithm are compared and analyzed.

4.1. Under Pulsed Discharge Conditions

We carried on the simulation experiment in MATLAB, using the AUKF algorithm to carry on the SOC estimation experiment under the pulsed discharge condition. Firstly, the initial values of the AUKF algorithm were set as follows: $x_0 = [0\ 0\ SOC]^T$,$P_0 = diag([10^{-5}, 10^{-5}, 10^{-3}])$, $W = 1180$, $Q = 10^{-7} \times eye(3)$, $R = 1$. Then, the AUKF algorithm was used to estimate the SOC under pulsed discharge conditions. The robustness of the proposed AUKF algorithm was tested under different initial SOC conditions. Finally, the results of SOC estimation using UKF algorithm and AUKF algorithm were compared and analyzed.

Experiments and analyses were performed under pulsed discharge conditions. For the initial SOC = 0.4, the comparison between the results estimated using the UKF algorithm and the AUKF algorithm is shown in Figure 14. For the initial SOC = 0.6, the comparison between the results estimated using the UKF algorithm and the AUKF algorithm is shown in Figure 15. For the initial SOC = 0.8, the comparison of the results estimated using the UKF algorithm and the AUKF algorithm is shown in Figure 16.

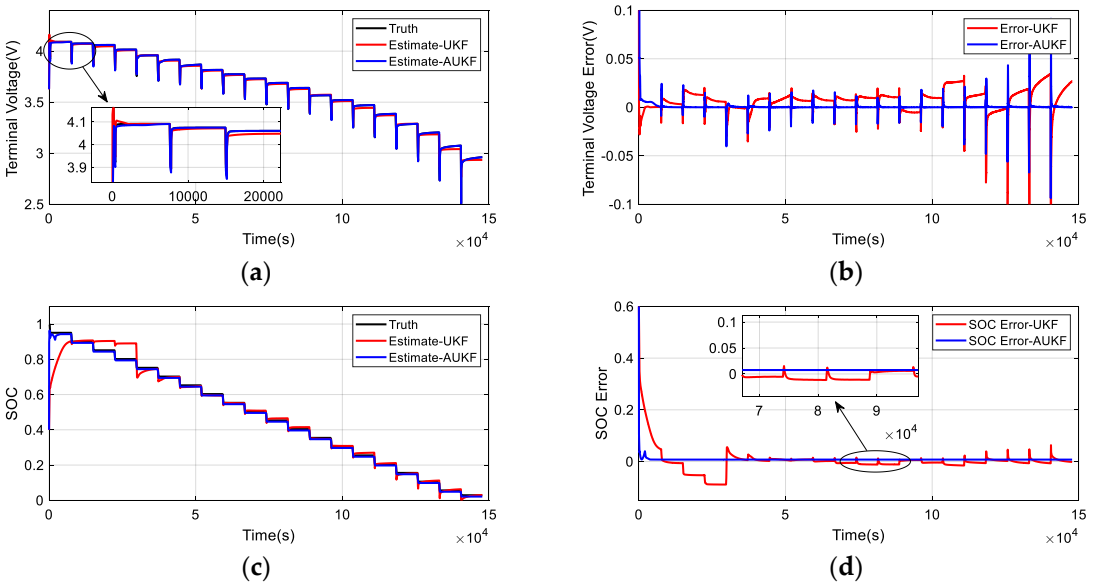

Figure 14. For the initial SOC = 0.4, the comparison of the estimation results of the UKF algorithm and the AUKF algorithm under pulsed discharge conditions. (**a**) Comparison of terminal voltage. (**b**) Comparison of terminal voltage errors. (**c**) Comparison of SOC. (**d**) Comparison of SOC errors.

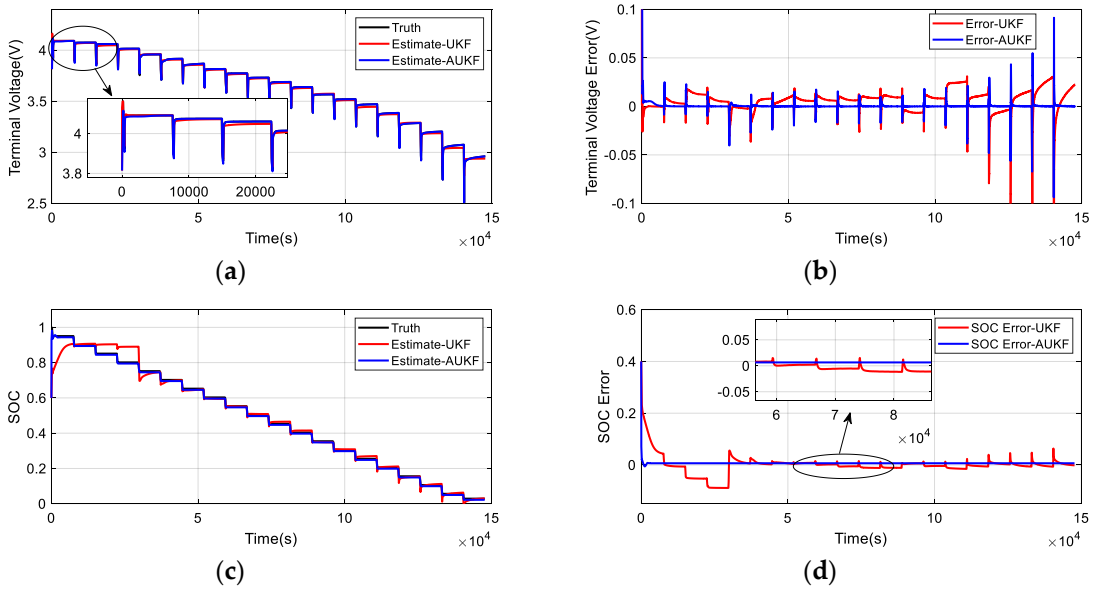

Figure 15. For the initial SOC = 0.6, the comparison of the estimation results of the UKF algorithm and the AUKF algorithm under pulsed discharge conditions. (**a**) Comparison of terminal voltage. (**b**) Comparison of terminal voltage errors. (**c**) Comparison of SOC. (**d**) Comparison of SOC errors.

From Figures 14a, 15a and 16a, it can be seen that under pulsed discharge conditions, the value of the battery terminal voltage estimated by the AUKF algorithm is closer to the true value than the value estimated by the UKF algorithm value. From Figures 14b, 15b and 16b, it can be seen that under pulsed discharge conditions, the terminal voltage error value estimated by the AUKF algorithm is smaller than the terminal voltage error value estimated by the UKF algorithm. Additionally, the error value of the terminal voltage estimated by the AUKF algorithm is relatively small. According to Figures 14c, 15c and 16c, it can be seen that the SOC value estimated using the AUKF algorithm is closer to the true value. From Figures 14d, 15d and 16d, it can be seen that the SOC estimation error of AUKF is smaller than that of UKF, and the convergence speed of AUKF algorithm is faster. In summary, under pulsed

discharge conditions and different initial SOC conditions, the robustness of the AUKF algorithm for estimating the SOC of the battery is better than that of the UKF algorithm.

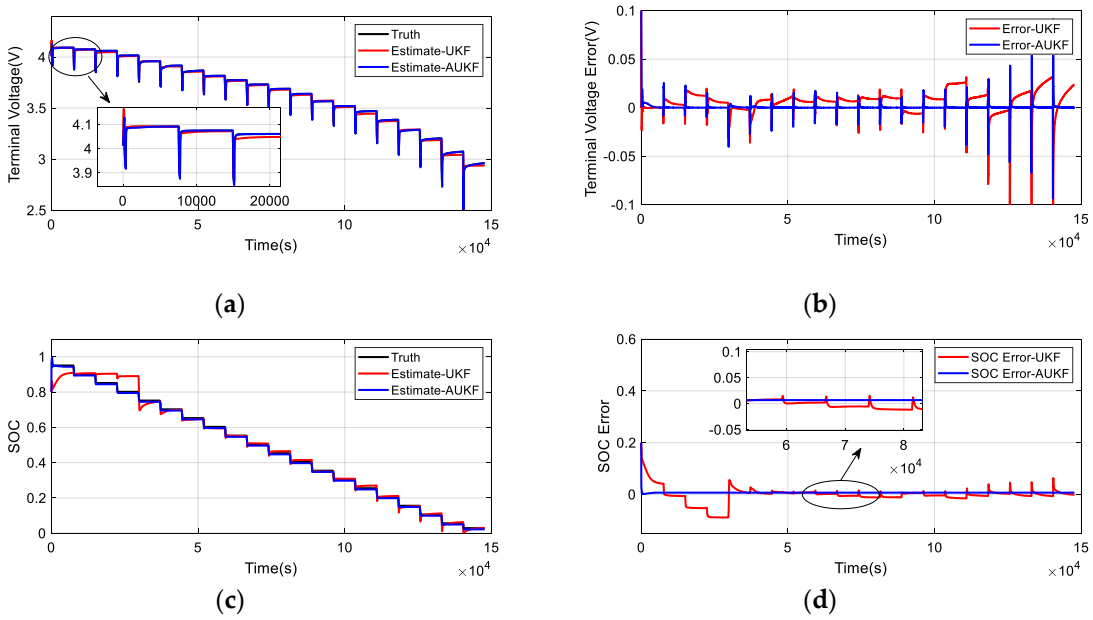

Figure 16. For the initial SOC = 0.8, the comparison of the estimation results of the UKF algorithm and the AUKF algorithm under pulsed discharge conditions. (**a**) Comparison of terminal voltage. (**b**) Comparison of terminal voltage errors. (**c**) Comparison of SOC. (**d**) Comparison of SOC errors.

4.2. Under UDDS Discharge Conditions

We carried on the simulation experiment in MATLAB, using AUKF algorithm to carry on the SOC estimation experiment under the UDDS discharge condition. Firstly, the initial values of the AUKF algorithm were set as follows: $x_0 = [0\ 0\ SOC]^T$, $P_0 = diag([10^{-5}, 10^{-5}, 10^{-3}])$, $W = 1180$, $Q = 10^{-7} \times eye(3)$, $R = 1$. Then, the AUKF algorithm was used to estimate the SOC under UDDS discharge conditions. The robustness of the proposed AUKF algorithm was tested under different initial SOC conditions. Finally, the results of SOC estimation using UKF algorithm and AUKF algorithm were compared and analyzed.

Experiments and analyses were performed under UDDS discharge conditions. For the initial SOC = 0.4, the comparison between the results estimated using the UKF algorithm and the AUKF algorithm is shown in Figure 17. For the initial SOC = 0.6, the comparison between the results estimated using the UKF algorithm and the AUKF algorithm is shown in Figure 18. For the initial SOC = 0.8, the comparison of the results estimated using the UKF algorithm and the AUKF algorithm is shown in Figure 19.

From Figures 17a, 18a and 19a, it can be seen that under UDDS discharge conditions, the value of the battery terminal voltage estimated by the AUKF algorithm is closer to the true value than the value estimated by the UKF algorithm. From Figures 17b, 18b and 19b, it can be seen that under UDDS discharge conditions, the terminal voltage error value estimated by the AUKF algorithm is smaller than the terminal voltage error value estimated by the UKF algorithm. Additionally, the error value of the terminal voltage estimated by the AUKF algorithm is relatively stable. According to Figures 17c, 18c and 19c, it can be concluded that the SOC value estimated using the AUKF algorithm is closer to the true value. From Figures 17d, 18d and 19d, it can be seen that the SOC estimation error of AUKF is smaller than that of UKF, and the convergence speed of AUKF algorithm is faster. In summary, under UDDS discharge conditions and under different initial SOC conditions, the robustness of the AUKF algorithm for estimating the SOC of the battery is better than the UKF algorithm.

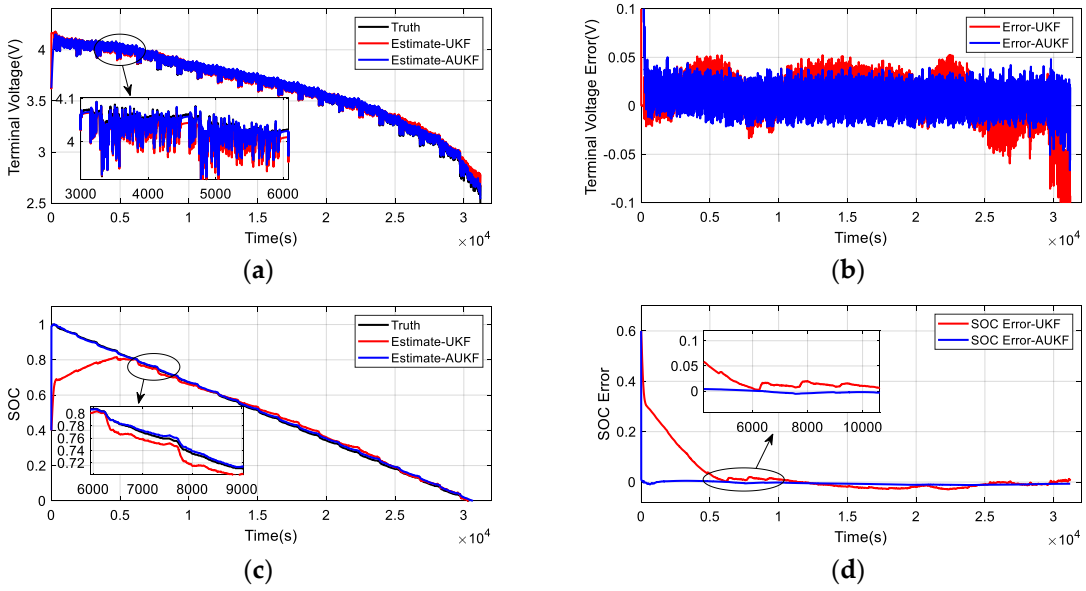

Figure 17. For the initial SOC = 0.4, the comparison of the estimation results of the UKF algorithm and the AUKF algorithm under UDDS discharge conditions. (**a**) Comparison of terminal voltage. (**b**) Comparison of terminal voltage errors. (**c**) Comparison of SOC. (**d**) Comparison of SOC errors.

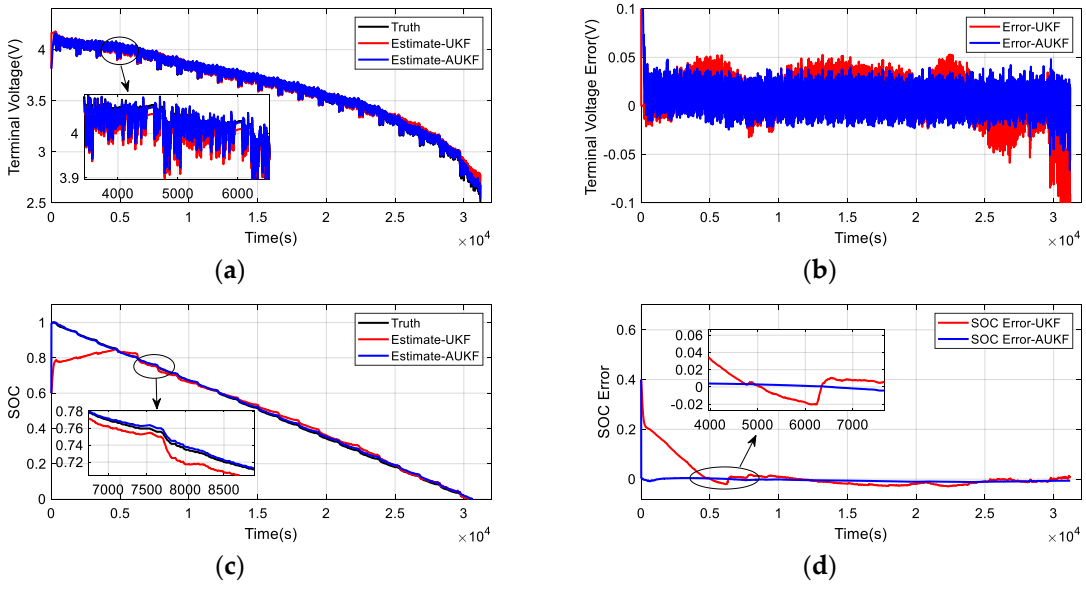

Figure 18. For the initial SOC = 0.6, the comparison of the estimation results of the UKF algorithm and the AUKF algorithm under UDDS discharge conditions. (**a**) Comparison of terminal voltage. (**b**) Comparison of terminal voltage errors. (**c**) Comparison of SOC. (**d**) Comparison of SOC errors.

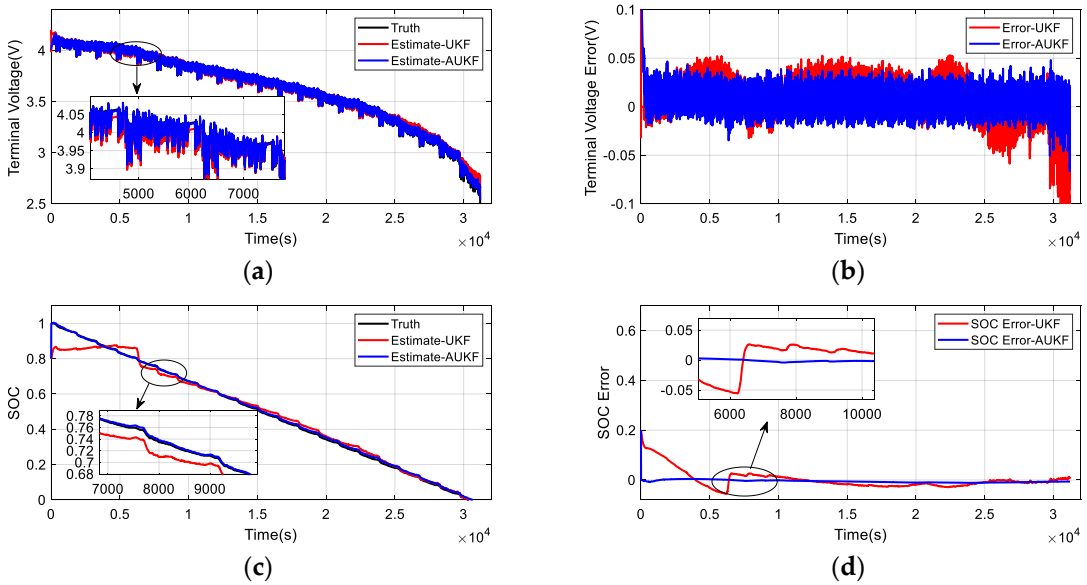

Figure 19. For the initial SOC = 0.8, the comparison of the estimation results of the UKF algorithm and the AUKF algorithm under UDDS discharge conditions. (**a**) Comparison of terminal voltage. (**b**) Comparison of terminal voltage errors. (**c**) Comparison of SOC. (**d**) Comparison of SOC errors.

In order to further verify the accuracy of the SOC estimation by the AUKF algorithm, the terminal voltage value and the SOC value estimated by the UKF algorithm and the AUKF algorithm were subjected to error analysis. The error results of the battery SOC estimation under different load cycles and different initial SOC values were averaged. The error analysis results of the terminal voltage are shown in Table 5. The error analysis results of the estimated SOC are shown in Table 6.

Table 5. Terminal voltage error.

Algorithm \ Error Type	MAE	RMSE
UKF	1.33%	1.95%
AUKF	0.54%	0.9%

Table 6. SOC error.

Algorithm \ Error Type	MAE	RMSE
UKF	2.9%	3.3%
AUKF	0.63%	0.7%

The mean absolute error (MAE) can avoid the problem of the deviations cancelling each other out, and can well describe the degree of data dispersion. The root mean square error (RMSE) measures the deviation between the observation value and the true value, and can well reflect the accuracy of the measurement. Table 5 shows that the MAE of the terminal voltage estimated by AUKF was smaller, indicating that the terminal voltage estimated by AUKF is less discrete than that of UKF algorithm; the RMSE of terminal voltage estimated by AUKF algorithm was smaller than that of UKF algorithm. Table 6 shows that the SOC value estimated by the AUKF algorithm had a smaller MAE than that of UKF algorithm. The RMSE of SOC estimated by AUKF algorithm was 2.6% smaller than that of UKF algorithm. The above error analysis results indicate that the accuracy of SOC estimation using AUKF algorithm is better than that of UKF algorithm.

5. Conclusions

In this paper, an adaptive unscented Kalman filter algorithm was designed to estimate the SOC of a lithium cobalt oxide battery. The second-order RC equivalent circuit model was used for nonlinear modeling of batteries. The least square method was used to identify the parameters of the battery model and for simulations in MALAB according to the battery voltage characteristics. The established model was verified under pulsed discharge conditions; the model error is 0.8%, which provides an accurate model for SOC estimation using AUKF algorithm. The system noise covariance Q value and observation noise covariance R value in the unscented Kalman filter algorithm were analyzed in this paper. The AUKF algorithm updates the system noise covariance Q and the observation noise covariance R in real time by monitoring the changes of the innovation and residual in the filter to adjust the filter gain and achieve the optimal estimate. The AUKF algorithm and UKF algorithm were used for SOC estimation under different load cycles and different initial SOC values. The estimated result of AUKF algorithm was more accurate, and the convergence rate of filtering was faster than that of UKF algorithm. To further verify the effectiveness of the AUKF algorithm, the estimated error of the terminal voltage and the estimated error of the SOC were analyzed. The error results show that the error of SOC estimation using AUKF algorithm was 0.7%, which was 2.6% smaller than that of SOC estimation using UKF algorithm.

Author Contributions: J.L. and X.W. proposed the innovative idea; J.L. conceived the algorithm and wrote the first draft; Y.L. improved the algorithm; J.L. performed the experiments; J.L. and X.W. analyzed the results; Y.F. and B.J. provided writing advice; J.L. approved the final manuscript. All authors have read and agreed to the published version of the manuscript.

Funding: The research received no external funding.

Acknowledgments: We gratefully acknowledge the technical assistance of DL850E ScopeCorder.

Conflicts of Interest: The authors declare no conflict of interest.

References

1. Gruosso, G.; Gajani, G.S.; Ruiz, F.; Valladolid, J.D.; Patino, D. A virtual sensor for electric vehicles' state of charge estimation. *Electronics* **2020**, *9*, 278. [CrossRef]
2. Yuan, W.; Jeong, S.; Sean, W.; Chiang, Y. Development of Enhancing Battery Management for Reusing Automotive Lithium-Ion Battery. *Energies* **2020**, *13*, 3306. [CrossRef]
3. Yang, Y.; Tan, Z.; Ren, Y. Research on factors that influence the fast charging behavior of private battery electric vehicles. *Sustainability* **2020**, *12*, 3439. [CrossRef]
4. Feng, F.; Teng, S.; Liu, K.; Xie, J.; Xie, Y.; Liu, B.; Li, K. Co-estimation of lithium-ion battery state of charge and state of temperature based on a hybrid electrochemical-thermal-neural-network model. *J. Power Sources* **2020**, *455*, 227935. [CrossRef]
5. Li, Y.; Chattopadhyay, P.; Xiong, S.; Ray, A.; Rahn, C.D. Dynamic data-driven and model-based recursive analysis for estimation of battery state-of-charge. *Appl. Energy* **2016**, *184*, 266–275. [CrossRef]
6. Chang, L.; Wang, C.; Zhang, C.; Xiao, L.; Cui, N.; Li, H.; Qiu, J. A novel fast capacity estimation method based on current curves of parallel-connected cells for retired lithium-ion batteries in second-use applications. *J. Power Sources* **2020**, *459*, 227901. [CrossRef]
7. Vo, T.T.; Chen, X.; Shen, W.; Kapoor, A. New charging strategy for lithium-ion batteries based on the integration of Taguchi method and state of charge estimation. *J. Power Sources* **2015**, *273*, 413–422. [CrossRef]
8. Chen, X.; Lei, H.; Xiong, R.; Shen, W.; Yang, R. A novel approach to reconstruct open circuit voltage for state of charge estimation of lithium ion batteries in electric vehicles. *Appl. Energy* **2019**, *255*, 113758. [CrossRef]
9. Stolze, C.; Hager, M.D.; Schubert, U.S. State-of-charge monitoring for redox flow batteries: A symmetric open-circuit cell approach. *J. Power Sources* **2019**, *423*, 60–67. [CrossRef]
10. Yang, F.; Li, W.; Li, C.; Miao, Q. State-of-charge estimation of lithium-ion batteries based on gated recurrent neural network. *Energy* **2019**, *175*, 66–75. [CrossRef]
11. Bian, C.; He, H.; Yang, S. Stacked bidirectional long short-term memory networks for state-of-charge estimation of lithium-ion batteries. *Energy* **2020**, *191*, 116538. [CrossRef]

12. Martino, L.; Read, J.; Elvira, V.; Louzada, F. Cooperative parallel particle filters for online model selection and applications to urban mobility. *Digit. Signal. Process.* **2017**, *60*, 172–185. [CrossRef]
13. Martino, L.; Elvira, V.; Camps-Valls, G. Group Importance Sampling for particle filtering and MCMC. *Digit. Signal. Process.* **2018**, *82*, 133–151. [CrossRef]
14. Mawonou, K.S.R.; Eddahech, A.; Dumur, D.; Beauvois, D.; Godoy, E. Improved state of charge estimation for Li-ion batteries using fractional order extended Kalman filter. *J. Power Sources* **2019**, *435*, 226710. [CrossRef]
15. Linghu, J.; Kang, L.; Liu, M.; Luo, X.; Feng, Y.; Lu, C. Estimation for state-of-charge of lithium-ion battery based on an adaptive high-degree cubature Kalman filter. *Energy* **2019**, *189*, 116204. [CrossRef]
16. Guo, F.; Hu, G.; Xiang, S.; Zhou, P.; Hong, R.; Xiong, N. A multi-scale parameter adaptive method for state of charge and parameter estimation of lithium-ion batteries using dual Kalman filters. *Energy* **2019**, *178*, 79–88. [CrossRef]
17. Zheng, Y.; Gao, W.; Ouyang, M.; Lu, L.; Zhou, L.; Han, X. State-of-charge inconsistency estimation of lithium-ion battery pack using mean-difference model and extended Kalman filter. *J. Power Sources* **2018**, *383*, 50–58. [CrossRef]
18. Tian, Y.; Lai, R.; Li, X.; Xiang, L.; Tian, J. A combined method for state-of-charge estimation for lithium-ion batteries using a long short-term memory network and an adaptive cubature Kalman filter. *Appl. Energy* **2020**, *265*, 114789. [CrossRef]
19. Partovibakhsh, M.; Liu, G. An adaptive unscented kalman filtering approach for online estimation of model parameters and state-of-charge of lithium-ion batteries for autonomous mobile robots. *IEEE Trans. Control. Syst. Technol.* **2015**, *23*, 357–363. [CrossRef]
20. Wang, S.; Fernandez, C.; Yu, C.; Fan, Y.; Cao, W.; Stroe, D.I. A novel charged state prediction method of the lithium ion battery packs based on the composite equivalent modeling and improved splice Kalman filtering algorithm. *J. Power Sources* **2020**, *471*, 228450. [CrossRef]
21. Pérez, G.; Garmendia, M.; Reynaud, J.F.; Crego, J.; Viscarret, U. Enhanced closed loop State of Charge estimator for lithium-ion batteries based on Extended Kalman Filter. *Appl. Energy* **2015**, *155*, 834–845. [CrossRef]
22. Smiley, A.; Plett, G.L. An adaptive physics-based reduced-order model of an aged lithium-ion cell, selected using an interacting multiple-model Kalman filter. *J. Energy Storage* **2018**, *19*, 120–134. [CrossRef]
23. Plett, G.L. Extended Kalman filtering for battery management systems of LiPB-based HEV battery packs—Part 2. Modeling and identification. *J. Power Sources* **2004**, *134*, 262–276. [CrossRef]
24. Plett, G.L. Extended Kalman filtering for battery management systems of LiPB-based HEV battery packs—Part 3. State and parameter estimation. *J. Power Sources* **2004**, *134*, 277–292. [CrossRef]
25. He, H.; Xiong, R.; Peng, J. Real-time estimation of battery state-of-charge with unscented Kalman filter and RTOS μCOS-II platform. *Appl. Energy* **2016**, *162*, 1410–1418. [CrossRef]
26. Sun, F.; Hu, X.; Zou, Y.; Li, S. Adaptive unscented Kalman filtering for state of charge estimation of a lithium-ion battery for electric vehicles. *Energy* **2011**, *36*, 3531–3540. [CrossRef]
27. Gustafsson, F.; Hendeby, G. Some relations between extended and unscented Kalman filters. *IEEE Trans. Signal. Process.* **2012**, *60*, 545–555. [CrossRef]
28. Chen, K.; Yu, J. Short-term wind speed prediction using an unscented Kalman filter based state-space support vector regression approach. *Appl. Energy* **2014**, *113*, 690–705. [CrossRef]
29. Lin, C.; Tang, A.; Xing, J. Evaluation of electrochemical models based battery state-of-charge estimation approaches for electric vehicles. *Appl. Energy* **2017**, *207*, 394–404. [CrossRef]
30. Ringbeck, F.; Garbade, M.; Sauer, D.U. Uncertainty-aware state estimation for electrochemical model-based fast charging control of lithium-ion batteries. *J. Power Sources* **2020**, *470*, 228221. [CrossRef]
31. Seaman, A.; Dao, T.S.; McPhee, J. A survey of mathematics-based equivalent-circuit and electrochemical battery models for hybrid and electric vehicle simulation. *J. Power Sources* **2014**, *256*, 410–423. [CrossRef]
32. Zhang, X.; Lu, J.; Yuan, S.; Yang, J.; Zhou, X. A novel method for identification of lithium-ion battery equivalent circuit model parameters considering electrochemical properties. *J. Power Sources* **2017**, *345*, 21–29. [CrossRef]
33. Bhattacharjee, A.; Roy, A.; Banerjee, N.; Patra, S.; Saha, H. Precision dynamic equivalent circuit model of a Vanadium Redox Flow Battery and determination of circuit parameters for its optimal performance in renewable energy applications. *J. Power Sources* **2018**, *396*, 506–518. [CrossRef]

34. Zhu, Q.; Xiong, N.; Yang, M.L.; Huang, R.S.; Di Hu, G. State of charge estimation for lithium-ion battery based on nonlinear observer: An H∞ method. *Energies* **2017**, *10*, 679. [CrossRef]
35. Piller, S.; Perrin, M.; Jossen, A. Methods for state-of-charge determination and their applications. *J. Power Sources* **2001**, *96*, 113–120. [CrossRef]
36. Zhang, Q.; Yang, Y.; Xiang, Q.; He, Q.; Zhou, Z.; Yao, Y. Noise Adaptive Kalman Filter for Joint Polarization Tracking and Channel Equalization Using Cascaded Covariance Matching. *IEEE Photonics J.* **2018**, *10*, 1–11. [CrossRef]
37. Song, M.; Astroza, R.; Ebrahimian, H.; Moaveni, B.; Papadimitriou, C. Adaptive Kalman filters for nonlinear finite element model updating. *Mech. Syst. Signal. Process.* **2020**, *143*, 106837. [CrossRef]